Rare Metal Materials and Engineering
Volume 47, Issue 5, May 2018
Online English edition of the Chinese language journal

Available online at www.sciencedirect.com
ScienceDirect

Cite this article as: Rare Metal Materials and Engineering, 2018, 47(5): 1385-1392.

ARTICLE

Evolution of Phase Microstructure and Properties of Mulit-core Cermets Based on (Ti,W,Ta)CN and TiCN Powders in Sintering Process

Wang Jie[1], Liu Ying[1,2], Ye Jinwen[1]

[1] Sichuan University, Chengdu 610065, China; [2] Key Laboratory of Advanced Special Material & Technology, Ministry of Education, Chengdu 610065, China

Abstract: The phase, microstructure and properties of multi-core cermets based on (Ti,W,Ta)CN and TiCN powders were investigated in sintering process. The analyses of X-ray diffraction (XRD) and scanning electron microscope (SEM) indicate that the sintering behavior of the multi-core cermet in sintering process could be divided into three stages: (I) pre-densification stage (the sintering temperature < 1200 °C); (II) rapid densification stage (the sintering temperature between 1200 °C and 1350 °C); (III) final densification stage (the sintering temperature > 1350 °C). Meanwhile, the evolution of η-phase in multi-core cermets was discussed as well. Furthermore, the microstructural and chemical composition of η-phase were studied by transmission electron microscopy (TEM) using X-ray energy dispersive spectrometry (XEDS) and selected area electron diffraction (SAED). The thickness of the rim structure would increase with the rise of sintering temperature, while the mechanical properties of the material would firstly increase and then decrease with the rise of sintering temperature. The highest transverse rupture strength is achieved at 1450 °C, while the highest hardness at 1390 °C.

Key words: TiCN-based cermets; multi-core cermets; sintering process; (Ti,W,Ta)CN solid solution

Due to the superior mechanical properties and chemical stability, TiCN based cermets have received increasing attention [1,2] and been introduced into the field of cutting tools especially in high speed milling, semi-finishing and finishing [3]. It is known that TiCN based cermets possess higher hardness, more excellent chemical stability, higher wear resistance and better oxidation resistance but less toughness than the commonly used WC-Co based hard metals[4-6]. Thus, most efforts were focused on improving their comprehensive mechanical properties[7].

Many researches had been done aiming at revealing the influence of carbide addition such as WC, Mo_xC and HfC[8,9], and the relevant reaction mechanism had been studied on the formation of core/rim structure based on dissolution-reprecipitation theory[10,11]. These efforts have achieved many positive results that laid the foundation of the follow-up studies. Recently, Choongkwon Park et al. [12,13] obtained a kind of TiCN-(Ti,W)C-based cermets with fairly high mechanical properties with hardness of about 14 GPa and fracture toughness of about 12.1 MPa·m$^{1/2}$. Moreover, the multi-core cermet based on TiCN and (Ti,W,Ta)CN powders was prepared and achieved decent mechanical properties as well[14]. These researches indicated multi-core cermet holds the potential for the high performance cermet synthesis. However, there is lack of reports on the sintering process of the multi-core cermets. In addition, although there were some reports about η-phase in WC-Co system[15-17], few studies of TiCN-based cermet have been reported with η-phase involved, which might have influence on the mechanical properties of the cermets[14]. In this study, we investigated the sintering process, including the evolution of phase, microstructure and properties, of multi-core cermets based on TiCN and (Ti,W,Ta)CN powders. Meanwhile, the microstructure and chemical

Received date: August 15, 2017
Foundation item: National Natural Science Foundation of China (51634006)
Corresponding author: Liu Ying, Ph. D., Professor, School of Materials Science and Engineering, Sichuan University, Chengdu 610065, P. R. China, Tel: 0086-28-85405536, E-mail: liuying5536@163.com

Copyright © 2018, Northwest Institute for Nonferrous Metal Research. Published by Elsevier BV. All rights reserved.

composition of η-phase were studied by TEM using XEDS-TEM and SAED. This research could provide guidance on the preparation of high performance TiCN-based cermets.

1 Experiment

The starting materials were laboratory synthesized (Ti, 20W, 15Ta)($C_{0.7}$,$N_{0.3}$) solid solution powders, Ti($C_{0.7}$,$N_{0.3}$) solid solution powders, and market purchased WC, TaC, Mo_2C, Co and Ni powders. And hereinafter in this paper, the (Ti, 20W, 15Ta)($C_{0.7}$,$N_{0.3}$) solid solution powders and the Ti($C_{0.7}$,$N_{0.3}$) solid solution powders will be designated as TWTCN and TiCN for short, respectively.

The nominal composition of cermets samples employed 27wt%TWTCN-27wt%TiCN-18wt%WC-9wt%Mo_2C-4wt%TaC-7.5wt%Co-7.5wt%Ni. The raw materials were ball milled with Φ10 mm WC-8Co alloy balls at a ball-to-powder mass ratio of 8:1 for 72 h. Here was shown in Fig.1 the SEM image and XRD pattern of ball milled raw materials. Then the cermets samples were obtained via pelletizing, compacting under a pressure of 120 MPa and finally sintering for 1.5 h. The sintering conditions were given in Table 1.

The mixed powders and the as-prepared cermets samples were characterized via X-ray diffraction (XRD) (DX-2700, China) with a Cu Kα radiation source and a scanning rate of 0.06°/s. Scanning electron microscopy (SEM) was employed for the microstructure observation in back-scattered electron (BSE) mode with a JSM-6490LV machine, and chemical composition was determined by energy-dispersive X-ray spectroscopy (EDS) equipped in SEM. Transmission electron microscopic (TEM) images and selected area electron diffraction (SAED) patterns were obtained on a 200 kV FE (field emission) analytical electron microscope (Libra 200FE). X-ray energy dispersive spectrometric (XEDS) analyses were carried out using the Oxford INCA detector coupled to the TEM. The linear shrinkage rates along length direction were measured by vernier caliper. The Vickers-hardness (HV) was measured with an indenter load of 30 kg on polished surfaces of cermets and transverse rupture strength (TRS) (20 mm span, 0.5 mm/min crosshead speed) was tested using a material test machine (Shimadzu AG-10TA).

Table 1 Sintering conditions of each cermet sample

Samples	Sintering temperature/°C	Sintering time /h
A	600	1.5
B	800	1.5
C	1000	1.5
D	1150	1.5
E	1200	1.5
F	1250	1.5
G	1300	1.5
H	1350	1.5
I	1390	1.5
J	1420	1.5
K	1450	1.5
L	1480	1.5

2 Results and Discussion

2.1 Phase evolution

The ball milled raw materials were characterized by XRD and the results are shown in Fig.1a. It could be clearly noted that the mixed powders consist of all the raw ingredients intactly. And the mixed powders were also observed by SEM and the image is shown in Fig.1b. It could be seen that the powders are well distributed with particle size less than several micrometers after ball milling. This indicates that no mechanical alloying takes place in the milling process. After sintering, all the cermets samples were investigated by XRD and the patterns (from samples A to H) are shown in Fig.2a. Fig.2b and Fig.2c are the enlargement of the characteristic peak (111) of Co/Ni and (440) of η-phase, in which the blue dash line and the red dash line represent the position of (440) peak of W_4Co_2C (PDF: 06-0611) and W_3Co_3C (PDF:27-1125), respectively.

According to the serial XRD patterns in Fig.2a, it is clearly illustrated that no reaction happens before the temperature reaches 800 °C (sample A and B), and the phase composition of the tested samples (sample A and B) is consistent with that of the ball milled powders (Fig.1a). When the sintering temperature rises to 1000 °C, the appearance of the η-phase could be identified in the XRD pattern C of Fig.2a. Except the occurrence of the η-phase in sample C, the rest of the constituents almost remain the same as sample A and B. With the temperature increasing to 1150 °C, except for slight amount of WC, the carbides (Mo_2C and TaC) in mixed powders could hardly be identified any more seen from the XRD pattern D of Fig.2a. And when the sintering temperature rises above 1200 °C, the composition of the sintered samples remains the same as sample E which consists of TiCN/(Ti,M)CN, Co/Ni and η-phase.

The (111) characteristic peaks of Co and Ni were actually separated in sample A and B from Fig.2b, and then combined to one in sample C with sintering temperature rising to 1000 °C. Otherwise, the diffraction peaks of Co/Ni shifted toward lower angle with increasing temperature, which might be caused by the increase content of the carbides solid solution in Co/Ni. As Co/Ni phase plays the role of bonding ceramic phases[18], this solid solution could promote the formation of liquid phase in sintering process, which could result in rapid sintering of the components[19]. Meanwhile, according to

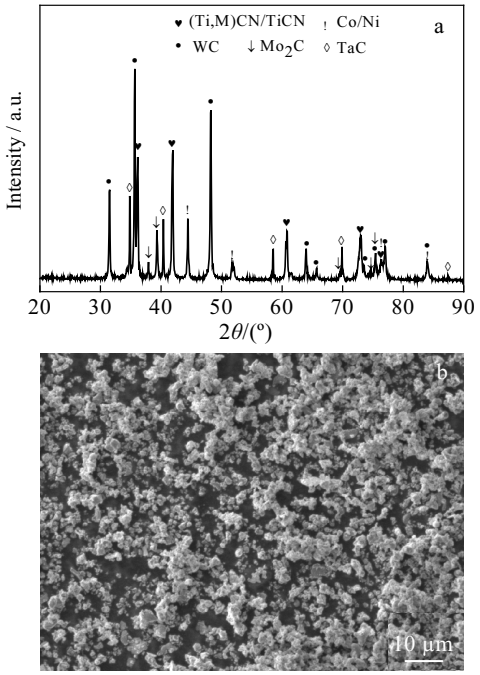

Fig.1 XRD pattern and SEM image of mixed raw materials

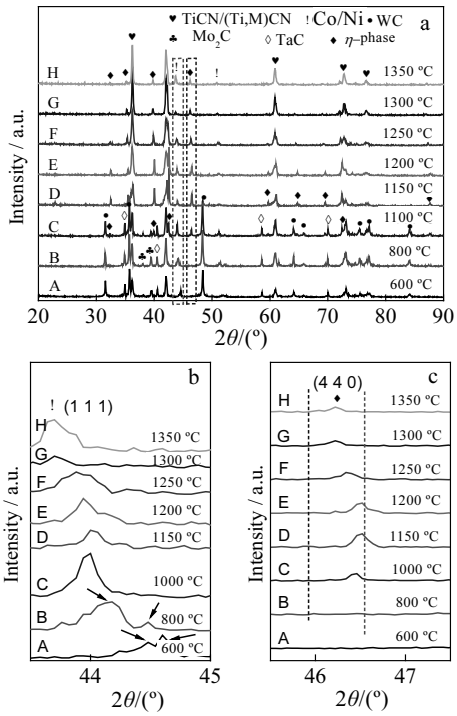

Fig.2 XRD patterns of sintered cermets from samples A to H (the blue dash line and red dash line are the (440) peaks of W_4Co_2C and W_3Co_3C, respectively)

Fig.2c it could be seen that the (440) characteristic peak of η-phase shifts to higher angle from η-phase emerging temperature 1000 °C to carbides disappearing temperature 1150 °C, which indicates the lattice constant of η-phase decreases in this period. Then the peak shifts back toward lower angle slightly when the temperature reaches 1200 °C and noticeably beyond 1200 °C, indicating the increase of lattice constant above 1200 °C. In Fig.2c, the relative intensity of (440) peaks of η-phase raises up firstly and then declines with increasing sintering temperature from 1000 °C to 1350 °C, in which the peak value is about 32% at 1200 °C. Generally, the relative intensity of XRD may be an assistant way to identify the phase content of the target material. It suggests that during the sintering process the formation of η-phase continues till the temperature rises to 1200 °C and then dissolution of η-phase commences when the temperature exceeds 1250 °C.

The XRD patterns of sample I to L are shown in Fig.3. The η-phase is detected in sample I and disappears in sample J, K and L, composed of (Ti, M)CN and Co/Ni, which indicates the dissolution of η-phase with elevating temperature.

The ternary phase diagram of W-Co-C system suggested that the WC-Co dual-phase region broaden while WC-Co-η three-phase region narrows down with temperature increasing[15,20]. With elevating temperature, it could lead to the dissolution of the lower temperature formed η-phase.

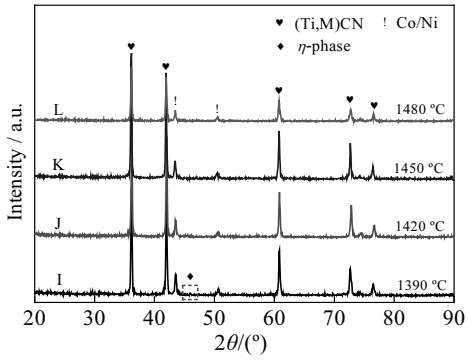

Fig.3 XRD patterns of sintered cermets from samples I to L

2.2 Microstructure

The SEM-BSE images of sample C to H, sintered from 1000 °C to 1350 °C as ascending order of temperature, are shown in Fig.4a to 4f. According to Fig.4a and 4b, granular structure could be obviously observed, which indicates no distinct sintering occurs among raw particles when the temperature is lower than 1150 °C. When the sintering temperature increases to 1200 °C, the amount of granular structure distinctly decreases and two kinds of core-structures, the grey core and black core, marked with black circle and black square in Fig.4c, respectively, could be clearly distinguished. The XEDS-TEM and SAED patterns of both core-structure in sample H are illustrated in Fig.5. The

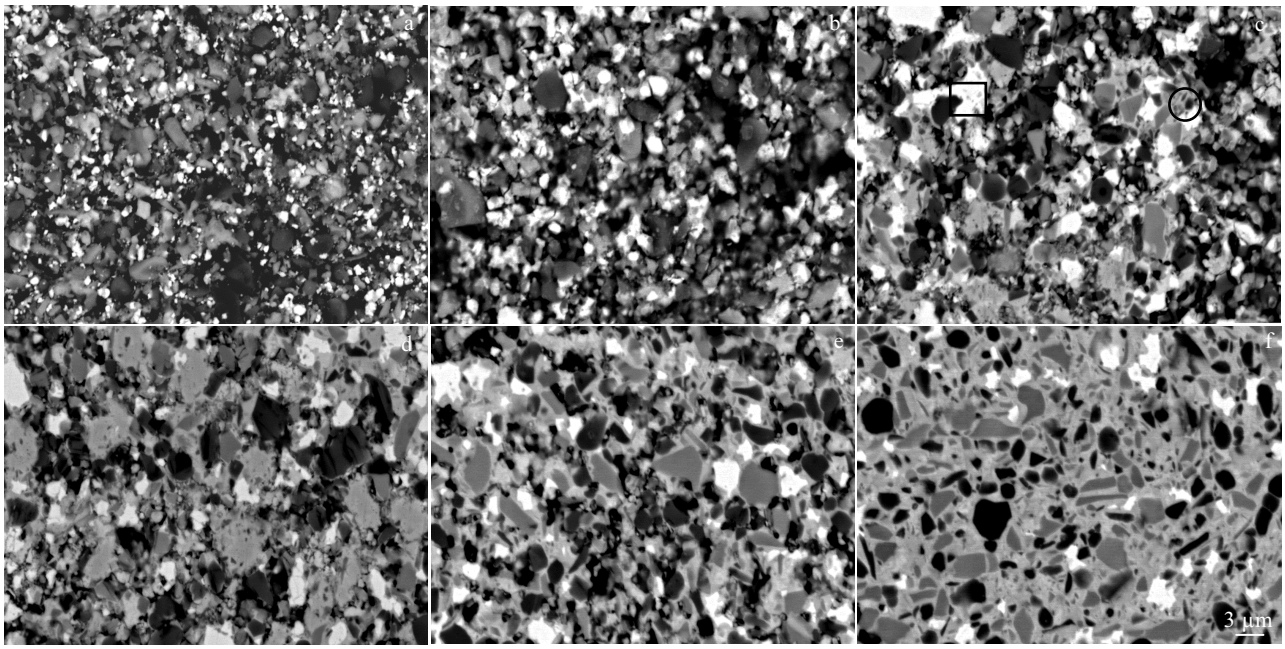

Fig. 4 SEM images of cermets from sample C to H (sintered from 1000 °C to 1350 °C): (a) sample C, (b) sample D, (c) sample E, (d) sample F, (e) sample G, and (f) sample H

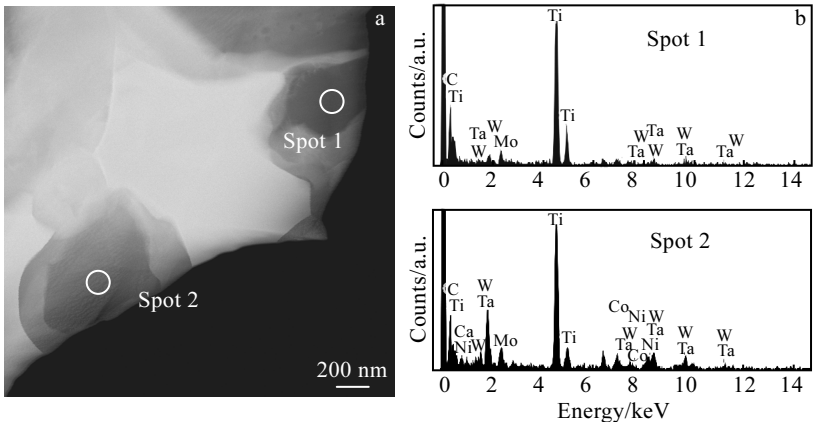

Fig.5 XEDS-TEM and SAED patterns of black core-structure and grey core-structure: (a) the TEM image of sample H, (b) the XEDS results of spot 1 and spot 2 in Fig.5a, (c, d) the SAED patterns of spot 1 and spot 2 in Fig.5a

obvious difference in chemical composition, mainly in W and Ta content, could be seen in Fig.5b. As the core-structure is the undissolved TiCN/(Ti,M)CN[11,21] phase, the core-structure around spot 1 and spot 2 in Fig.5a may be the undissolved TiCN and TWTCN, respectively. Furthermore, Fig.5c and 5d show the SAED patterns oriented along the [123] zone axe of Spot 1 and [114] zone axe of spot 2, respectively, indicating these two kinds of core-structures share the same cubic structure with TiCN. With sintering temperature increasing, whether core-structure or others, such as binder and white particles, become more integrated and coherent, indicating the sintering become sharper.

Meanwhile, according to Fig.4, the evolution of the white particles is noteworthy. They are tiny and dispersive when the cermet is sintered at 1000 °C in Fig.4a. While the sintering temperature increases to 1200 °C, the white particles in Fig.4c seem to be more aggregated and coarser than those in lower temperature sintered samples. Then it gets refined and gradually diminished with the increase of sintering temperature, which could well accord with the variation tendency of η-phase in Fig.2, suggesting the possible relationship between the white particle and the η-phase.

To investigate the microstructural and chemical information of the white particles, sample H was studied by TEM using XEDS-TEM and SAED (Fig.6). The (W,Mo,Ti)/(Co,Ni) atomic ratio of white particle is approximately 3.4/2.6 from the EDS results of the zone marked with white circle in Fig.6a, indicating the atomic ratio of the white particle falls in the range between that of W_4Co_2C and W_3Co_3C. Considering that W and Mo have similar atom radius, the mutual replacement of W and Mo may occur. The similar result could also be referred to the study conducted by N. Liu et al. [22]. The much less content of Ti compared to W and Mo in white particle implies the difficult dissolution of Ti into it, which could be derived from the larger difference of atom radius of Ti comparing with W and Mo. Furthermore, J. Kim et al. demonstrated that W_4Co_2C shares the same crystal structure with W_3Co_3C[23,24], indicating that W atom could replace Co atom without altering the crystal structure of W_4Co_2C and W_3Co_3C.

The SAED patterns of white particle (in Fig.6a) oriented along the [125] zone axe is shown in Fig.6b, which indicates the white particle has a cubic structure that

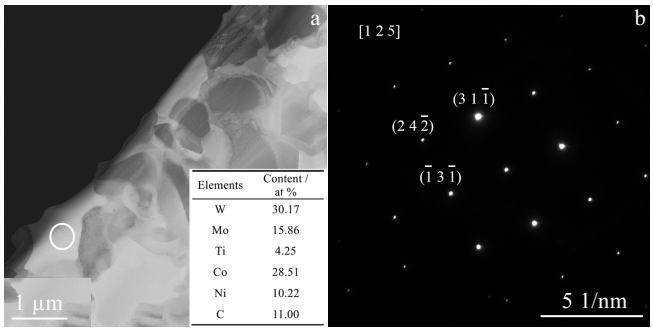

Fig.6 XEDS-TEM and SAED patterns of white particle in sample H: (a) TEM image and XEDS results and (b) SAED pattern of white circle zone in Fig. 6a

is totally identical with W_4Co_2C and W_3Co_3C phase. The results demonstrate the white particle formed in cermet could be η-phase that is a kind of continuous solid solution and could be expressed as $(W,Mo,Ti)_{3+x}(Co,Ni)_{3-x}C$ ($0<x\leq1$).

The chemical composition of the white particles from sample C to H (corresponding to Fig.4a to 4f, respectively) was measured on the polished samples by EDS linked with SEM in BSE mode, which are listed in Table 2. The contents of Co and Ni in white particles distinctly increase from 11.03 at% for Co and 7.74 at% for Ni in sample C to 27.58 at% for Co and 12.23 at% for Ni in sample D, respectively. This indicates that the solubility of Co and Ni in white particles increases a lot when sintering temperature rises from 1000 °C to 1150 °C. Therefore, in XRD measurement the higher angle shifting of the (440) peak of η-phase from 1000 °C sintered sample to 1150 °C sintered sample in Fig.2 could result from the increased number of Co and Ni atoms dissolved in, causing the decrease of (W, Mo,Ti)/(Co,Ni) atomic ratio, and leading to the lattice constant of η-phase close to that of W_3Co_3C. With increasing sintering temperature, the (W,Mo,Ti)/(Co,Ni) atomic ratio increases from 3.50/2.50 at 1200 °C (sample E) to 3.59/2.41 at 1250 ˚C (sample F) and then to 3.68/2.32 at 1350 °C (sample H), which may be the reason that the (440) peaks of η-phase shifts toward lower angle direction above 1250 °C in the XRD patterns as the (W,Mo,Ti)/(Co,Ni) atomic ratio in η-phase approaches to W_4Co_2C.

Table 2 Relative atomic content of white particles in different sintering conditions samples by EDS in Fig.4a~4f

Samples	Sintering temperature/°C	Relative atomic content/at%						
		W	Mo	Ti	Ta	Co	Ni	C
C	1000	45.16	-	33.92	-	11.03	7.74	2.15
D	1150	34.6	16.05	6.17	-	27.58	12.23	3.36
E	1200	34.66	16.53	4.91	-	28.08	12.16	3.66
F	1250	34.03	16.84	7.13	-	27.5	11.37	3.12
G	1300	33.13	17.75	6.9	-	26.2	10.85	5.17
H	1350	32.35	16.77	7.91	-	26.42	9.6	6.96

The BSE images of sample I to L are shown in Fig.7. It could be seen that the rim structure thickened gradually with elevating sintering temperature form 1390 °C to 1480 °C. Since the high sintering temperature would benefit the formation of liquid phase, which could promote the solution and precipitation process of cermet and then facilitate the formation of rim-structure in sintering process. Meanwhile, we can see the appearance of a small amount of tiny white particles (marked with white circle in Fig.7a) in sample I. While in Fig.7b, 7c and 7d (corresponding to sample J, K and L, respectively), no occurrence of white particles could be identified, indicating the complete dissolution of η-phase into the cermet system.

2.3 Mechanical characterization

The appearance of fracture surfaces from samples D to L is shown in Fig.8 and the linear shrinkages along length direction of sintered cermets are illustrated in Fig.9. It could be seen that the fracture surface of sample D and E (Fig.8a and 8b) is granular and porous, which indicates no obvious sintering occurring and nearly no shrinkage is found below 1200 °C. The analogue of sintering neck (marked with white circles in Fig.8d) could be noticed in

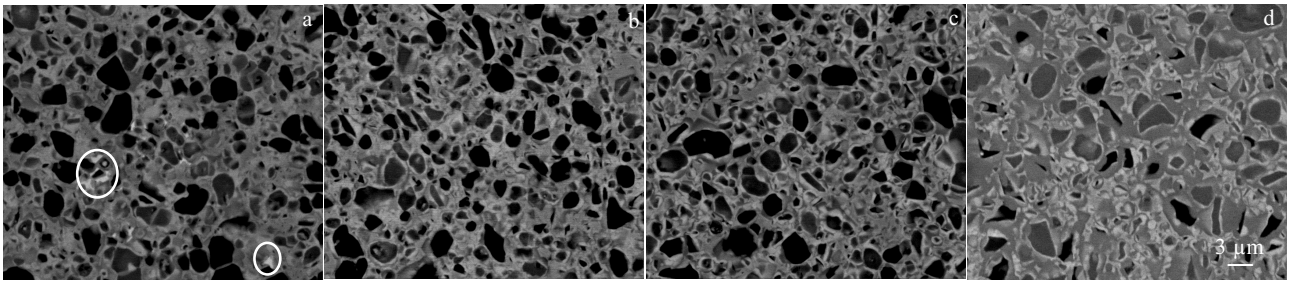

Fig.7 SEM images of cermet from sample I to L (sintered from 1390 °C to 1480 °C): (a) sample I, (b) sample J, (c) sample K, and (d) sample L

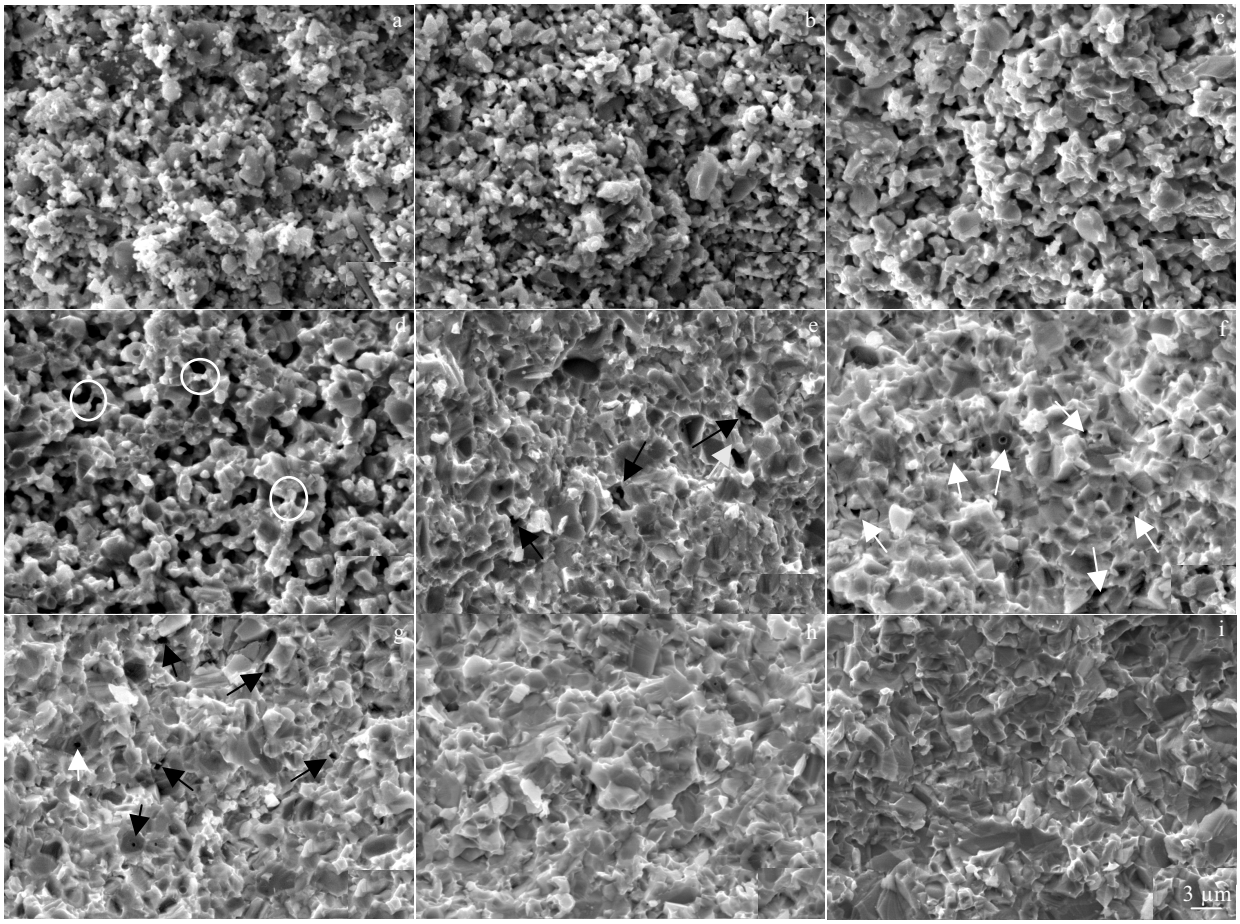

Fig.8 Appearance of fracture surfaces from sample D to L (sintering temperature from 1150 °C to 1480 °C): (a) sample D, (b) sample E, (c) sample F, (d) sample G, (e) sample H, (f) sample I, (g) sample J, (h) sample K, and (i) sample L

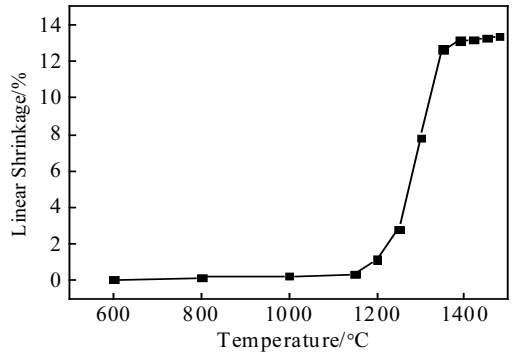

Fig.9 Linear shrinkage along length direction with sintering temperature increasing

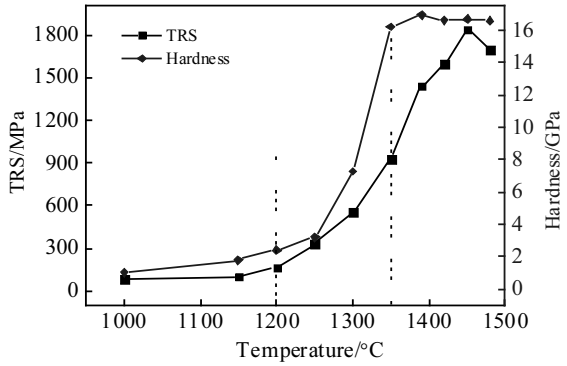

Fig.10 TRS and hardness of sintered cermets with sintering temperature increasing

sample G (sintered at 1300 °C), which indicates the occurrence of sintering results in the sharp contraction of cermet clearly shown in Fig.9. The number of pores decreases obviously when the sintering temperature reaches 1350 °C, and then decreases gradually (marked with black arrows in Fig.8e to 8g) with temperature rising to 1420 °C. The pores could be hardly observed when sintering temperature is raised to 1450 °C, which suggests that nearly all the pores get filled by the liquid phase after 1450 °C. At this stage, the comparatively low porosity could result in the shrinkage plateau stage after 1350 °C in Fig.9. Meanwhile, the slowing increase of shrinkage after 1350 °C could be attributed to the gradual filling of pores between each structure with the rising temperature. This result is in a good agreement with the previous reports[11] and about the liquid phase and shrinkage for TiCN based cermets[25].

Mechanical properties of the cermets at room temperature are shown in Fig.10. It could be seen from Fig.10 that both transverse rupture strength (TRS) and Vickers hardness exhibit slow increase initially prior to an abrupt increase above 1250 °C. TRS reaches the peak value in sample K (sintered at 1450 °C) before decrease, while hardness reaches the peak value in sample I (sintered at 1390 °C) before its slow decrease. Based on the discussion above, the increase of TRS and hardness at earlier stage could be ascribed to the densification of the cermet. On the other hand, the rising of TRS could be also attributed to the integrating of rim structure. And the increase of hardness would benefit from the reduction of η-phase which has low hardness about 12 GPa[23]. I. Konyashin et al.[26] reported that the transverse rupture strength of TiCN-based cermets would decrease obviously if the average thickness of the rim exceeded 0.5 μm. From Fig.7d, it could be seen that the most of the rim-structures of sample L were thicker than 0.5 μm, resulting in its TRS declining. The highest hardness of sample I could be ascribed to its relatively high densification and fine grain size. As to the slight drop of the hardness after 1390 °C, it may be caused by the grain growth with rising temperature, which would be harmful to hardness.

3 Conclusions

1) The multi-core cermet is prepared from 27wt%TWTCN-27wt%TiCN-18wt%WC-9wt%Mo_2C-4wt%TaC -7.5wt%Co-7.5wt%Ni. The sintering process of multi-core cermet could be approximately divided into three stages: (I) pre-densification stage (the sintering temperature < 1200 °C), during which the secondary carbides (Mo_2C, TaC and WC) gradually dissolve and the ceramics show poor density and mechanical properties. (II) rapid densification stage (the sintering temperature between 1200 °C and 1350 °C), during which the rim-structure begins to form and the ceramics shows obviously improved density and mechanical properties in this stage; (III) final densification stage (the sintering temperature > 1350 °C), during which the pores in ceramics get filled by the liquid phase, making the material gradually approach complete densification. And the and thickness of the rim-structure would increase with the rise of sintering temperature, while the mechanical properties of the material would firstly increase and then decrease with the rise of sintering temperature and achieve the highest TRS at 1450 °C, and the highest hardness at 1390 °C.

2) The content of η-phase increases with elevating sintering temperature from 1000 °C to 1200 °C, and then dissolves with further increase of sintering temperature till completely dissolves at 1420 °C. The η-phase formed in multi-core cermets is a kind of continuous solid solution and expressed as $(W,Mo,Ti)_{3+x}(Co,Ni)_{3-x}C$ ($0<x\leq1$) whose (W,Mo,Ti)/(Co,Ni) atomic ratio is between that of W_4Co_2C and W_3Co_3C phase having a cubic structure.

References

1 Zackrisson J, Andren H O. *International Journal of Refractory Metals and Hard Materials*[J], 1999, 17(4): 265

2 Moskowitz D, Terner L L. *Materials Science and Engineering*

A[J], 1988, 105-106(1): 265
3 Clark E B, Roebuck B. *International Journal of Refractory Metals and Hard Materials*[J], 1992, 11(1): 23
4 Wen G, Li S B, Zhang B S *et al*. *Acta Materialia*[J], 2001, 49(8): 1463
5 Vallauri D, Deorsola F A. *Materials Research Bulletin*[J], 2009, 44(7): 1528
6 Shobu K, Watanabe T, Enomoto Y *et al*. *Journal of the American Ceramic Society*[J], 1987, 70(5): C103
7 Jin Y Z, Liu Y, Wang Y K *et al*. *International Journal of Refractory Metals and Hard Materials*[J], 2009, 27(6): 957
8 Gao J J, Song J P, Liang G X *et al*. *Ceramics International*[J], 2017, 43(17): 14 945
9 Liu N, Xu Y D, Li Z H *et al*. *Ceramics International*[J], 2003, 29(8): 919
10 Li P P, Ye J W, Liu Y *et al*. *International Journal of Refractory Metals and Hard Materials*[J], 2012, 35: 27
11 Ahn S Y, Kang S. *Journal of the American Ceramic Society*[J], 2000, 83(6): 1489
12 Park C, Nam S, Kang S. *Journal of Alloys and Compounds*[J], 2016, 657: 671
13 Park C, Nam S, Kang S. *Materials Science and Engineering: A*[J], 2016, 649: 400
14 Wang J, Liu Y, Ye J W *et al*. *International Journal of Refractory Metals and Hard Materials*[J], 2017, 64: 294
15 de Villiers Lovelock H L. *Journal of Thermal Spray Technology*[J], 1998, 7(3): 357
16 Uskova S G, Shvetsova G A. *Soviet Powder Metallurgy and Metal Ceramics*[J], 1991, 30(10): 896
17 Kreimer G S, Vakhovskaya M R. *Soviet Powder Metallurgy and Metal Ceramics*[J], 1965, 4(6): 454
18 Xu Q Z, Ai X, Zhao J *et al*. *Journal of Alloys and Compounds*[J], 2015, 644: 663
19 Córdoba J M, Chicardi E, Gotor F J. *Journal of Alloys and Compounds*[J], 2013, 559: 34
20 Kurlov A S, Gusev A I. *Russian Chemical Reviews*[J], 2006, 75(7): 617
21 Chen L, Lengauer W, Ettmayer P *et al*. *Journal of Refractory Metals and Hard Materials*[J], 2000, 18(6): 307
22 Liu N, Liu X S, Zhang X B *et al*. *Materials Characterization*[J], 2008, 59(10): 1440
23 Kim J, Suh Y J, Kang I. *Journal of Alloys and Compounds*[J], 2016, 656: 213
24 Suetin D V, Medvedeva N I. *Journal of Alloys and Compounds*[J], 2016, 681: 508
25 Yang J K, Lee H C. *Materials Science and Engineering A*[J], 1996, 209(1): 213
26 Konyashin I. *International Journal of Refractory Metals and Hard Materials*[J], 2001, 19(4-6): 523

基于 TiCN 和(Ti,W,Ta)CN 的混芯结构金属陶瓷冶金过程中物相、组织结构及力学性能演变

王 杰[1], 刘 颖[1,2], 叶金文[1]
(1. 四川大学，四川 成都 610065)
(2. 教育部先进特种材料及制备加工技术重点实验室，四川 成都 610065)

摘 要：研究了基于 TiCN 和(Ti,W,Ta)CN 的混芯结构金属陶瓷冶金过程中的物相、组织结构和力学性能。通过 X 射线衍射（XRD）和扫描电子显微镜（SEM）等分析手段，研究了“混芯结构”金属陶瓷的冶金行为，其大致可以分为 3 个阶段：(I) 前致密化阶段，烧结温度低于 1200 ℃；(II) 快速致密化阶段，烧结温度在 1200~1350 ℃；(III) 最终致密化阶段，烧结温度高于 1350 ℃。同时，还讨论了 η 相在“混芯结构”金属陶瓷中的演变规律，并采用透射电子显微镜（TEM）中的 X 射线能量分光谱（XEDS）和选区电子衍射(SAED)等手段分析了其结构和化学成分。此外，随烧结温度增加，金属陶瓷中的环形结构会逐渐增厚，材料的力学性能呈先增加后降低的趋势。在烧结温度达到 1450 ℃时，材料具有最大的抗弯强度；而在烧结温度为 1390 ℃时，材料具有最大的硬度。

关键词：TiCN 基金属陶瓷；混芯结构金属陶瓷；烧结过程；（Ti, W, Ta）CN 固溶体

作者简介：王 杰，男，1988 年生，博士，四川大学材料科学与工程学院，四川 成都 610065，E-mail: 245552855@qq.com